Template-directed *in situ* grown bimetallic nanoarchitectures with hydroxide active sites enriched multi-charge transfer routes for energy storage

Antonysamy Dennyson Savariraj[a], Pugalenthiyar Thondaiman[b], Periyasamy Sivakumar[a], Ramu Manikandan[c], John D Rodney[b], Byung Chul Kim[b], Hyun Jung[a*].

[a] Advanced Functional Nanohybrid Material Laboratory, Department of Chemistry, Dongguk University Seoul-Campus, Jung-gu, Seoul 04620, Republic of Korea.

[b] Department of Advanced Components and Materials Engineering, Sunchon National University, 255, Jungang-ro, Suncheon-si, Jellanamdo 57922, Republic of Korea.

[c] Department of Energy and Materials Engineering, Dongguk University Seoul-Campus, Jung-gu, Seoul 04620, Republic of Korea.

*Corresponding Author: chemphile@dongguk.edu (Hyun Jung)

1. Equations:

The areal capacity (C_a) ($mC\ cm^{-2}$) of the electrodes can be calculated from the GCD curves using the following equation:.

$$C_a = \frac{I \times \Delta t}{a} \quad \text{(S1)}$$

Where I represents the discharge current (mA), Δt denotes discharge time (s) and a stands for the active area of the electrode (cm^2).

The specific capacity (C_s) (A g^{-1}) of the electrodes using a three-electrode system can be determined from the GCD curves by applying the variables in the following equation.

$$C_s = \frac{I \times \Delta t}{m} \quad \text{(S2)}$$

Here, I denotes discharge current (mA), Δt stands for the discharge time (s) and m is the mass of the electrode (mg).

The specific capacitance (C_{sp}) (F g^{-1}) can be calculated using the following equation:.

$$C_{sp} = \frac{I \times \Delta t}{\Delta V \times m} \quad \text{(S3)}$$

Where I is the discharge current (mA), Δt is the discharge time (s), ΔV denotes the potential window (V) and m represents the mass of the active material on the electrode (mg).

The volumetric capacitance (C_{vc}) (F cm^{-3}) of the electrodes can be determined using the following equation:.

$$C_{vc} = \frac{Specific\ capacitance}{Density} \quad \text{(S4)}$$

$$i = av^b \quad \text{(S5)}$$

$$\log i = \log a + b\ log v \quad \text{(S6)}$$

The equations S5 and S6 i and υ represent the current (A) and the scan rate (V s^{-1}) respectively, while *a* denotes the variable and *b* is the slope.

$$i(V) = K_1 v + K_2 v^{1/2} \quad \text{(S7)}$$

In the above equation, *i(V)* represents the potential dependent current, $K_1\upsilon$ is the surface capacitive contribution, and $K_2\upsilon^{1/2}$ is the diffusion-controlled contribution. The equation S7 can be rewritten and represented as follows to get the values of K_1 and K_2.

$$\frac{i(V)}{v^{1/2}} = K_1 v^{1/2} + K_2 \quad \text{(S8)}$$

The optimal mass ratio between positive and negative electrodes to assemble the hybrid asymmetric supercapacitor can be calculated using the following equation:.

$$\frac{m_+}{m_-} = \frac{C_- \times \Delta V_-}{C_+} \quad \text{(S9)}$$

Where 'm_+' and 'm_-', denote the active mass of positive and negative electrodes while 'C_+' and 'C_-', stand for the specific capacity of positive and negative electrodes respectively, and the voltage window of negative electrodes is represented by 'ΔV_-'.

The energy (E_s) and power (P_s) densities are the quintessential parameters of an asymmetric device, and these parameters can be calculated using the following equations (S10 and S11).

$$E_s = \frac{I \times \int V(t)dt}{m \times 3.6} \quad \text{(S10)}$$

$$P_s = \frac{E_s \times 3600}{t} \quad \text{(S11)}$$

Here, E_s stands for specific energy (Wh kg^{-1}), P_s represents the specific power (W kg^{-1}), and $\int V(t)dt$ denotes the integral area of the GCD curve.

2.Figures:

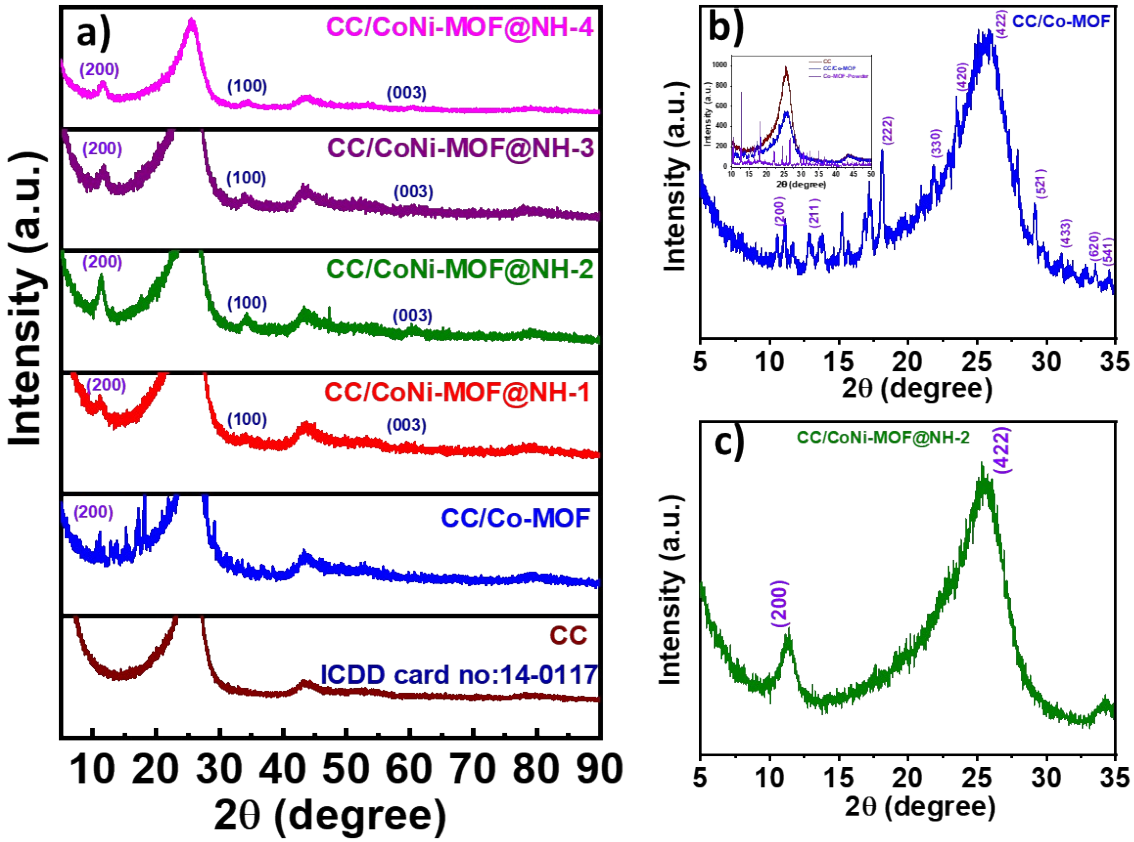

Figure S1. High magnification XRD patterns: (a) CC, CC/Co-MOF, CC/CoNi-MOF@NH-1, CC/CoNi-MOF@NH-2, CC/CoNi-MOF@NH-3, and CC/CoNi-MOF@NH-4 electrodes, (b) CC/Co-MOF electrode (inset shows the high magnification of CC, CC/Co-MOF electrode, and Co-MOF-powder sample), and (c) CC/CoNi-MOF@NH-2 electrode.

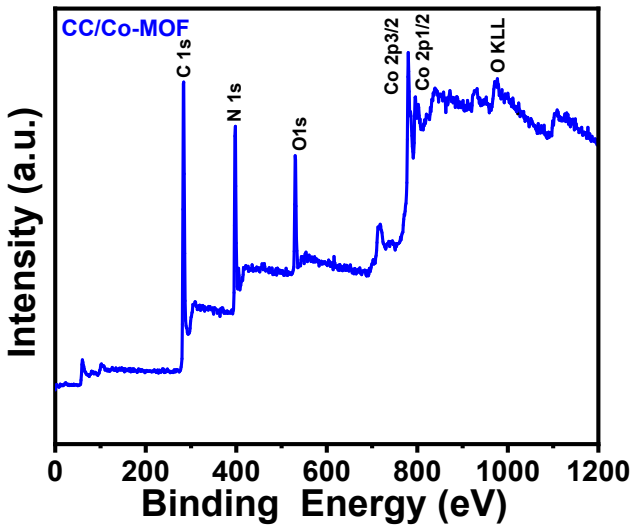

Figure S2. XPS survey spectra of the CC/Co-MOF electrode.

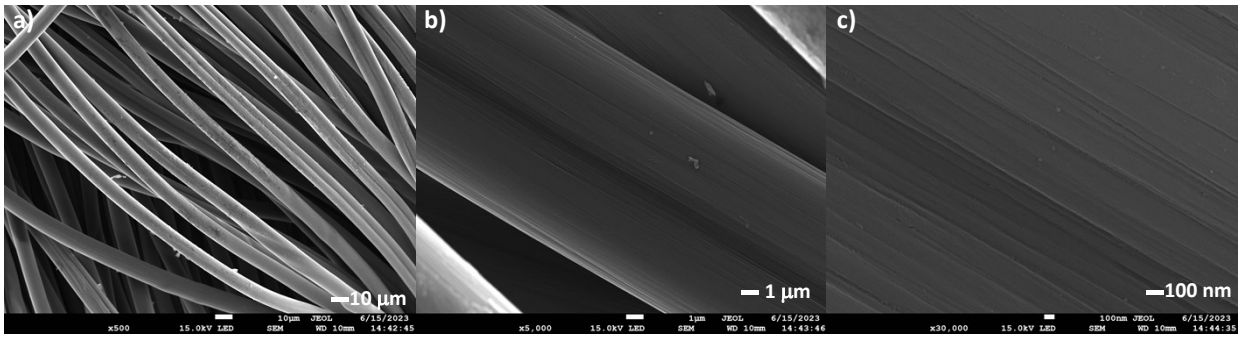

Figure S3. SEM images of bare carbon cloth (CC) at different magnifications.

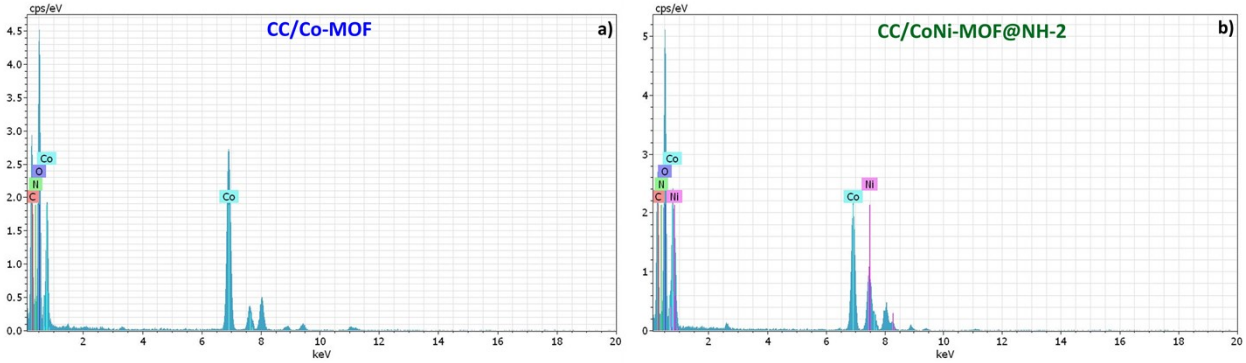

Figure S4. HRTEM energy-dispersive X-ray (EDX) spectrum of (a) CC/Co-MOF and (b) CC/CoNi-MOF@NH-2 electrodes.

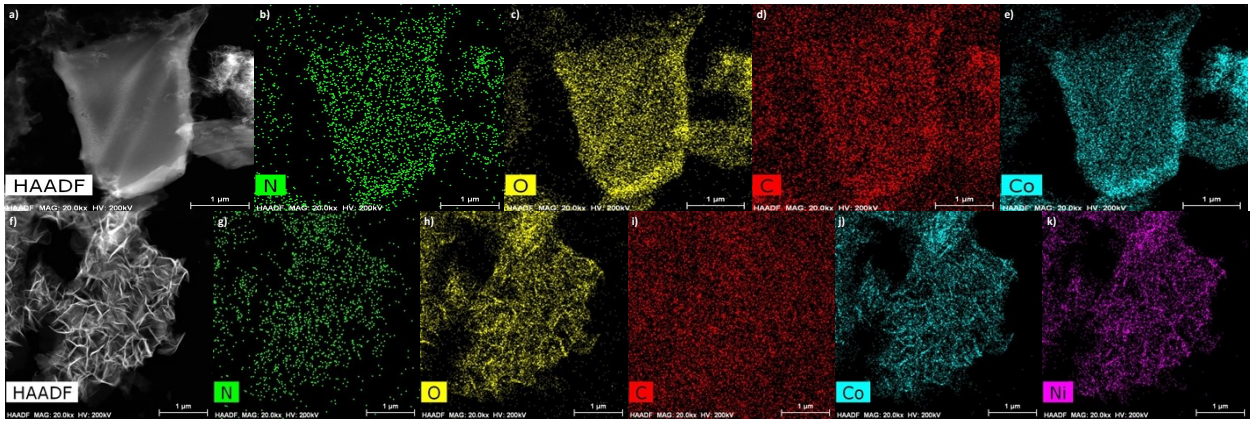

Figure S5. HRTEM EDX elemental mapping images of CC/Co-MOF: (a)-(e) and CC/CoNi-MOF@NH-2: (f)-(k) electrodes

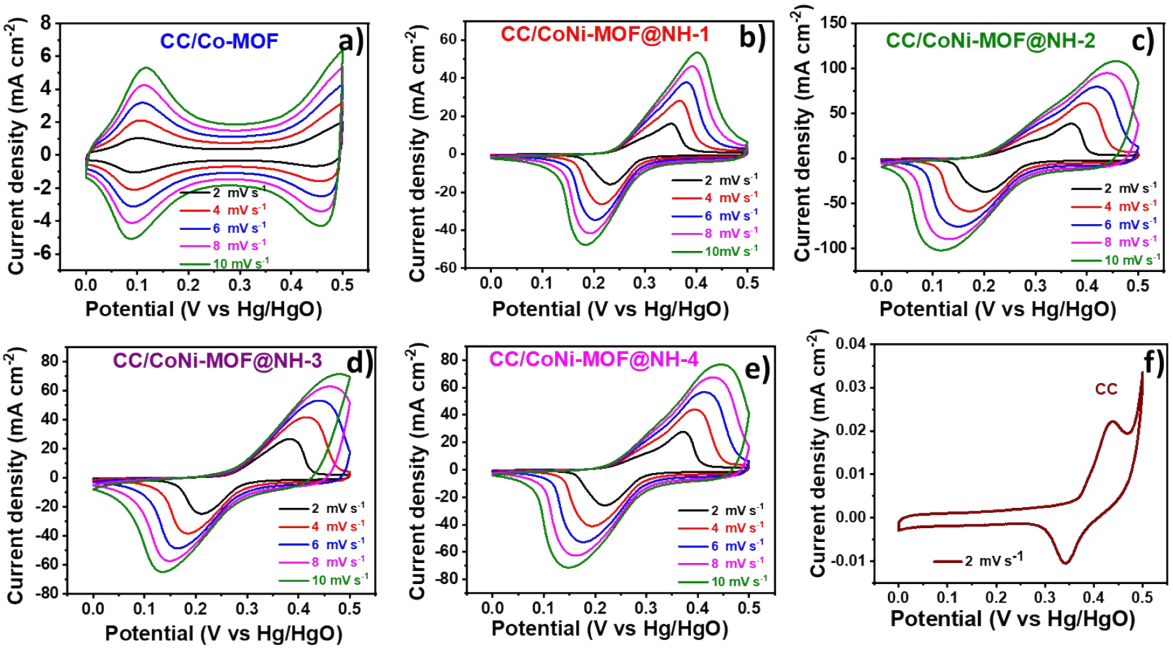

Figure S6. CVs measured at different scan rates for (a) CC/Co-MOF, (b) CC/CoNi-MOF@NH-1, (c) CC/CoNi-MOF@NH-2, (d) CC/CoNi-MOF@NH-3, and (e) CC/CoNi-MOF@NH-4 electrodes at different scan rates, and (f) CV of CC at a scan rate of 2 mV s^{-1}.

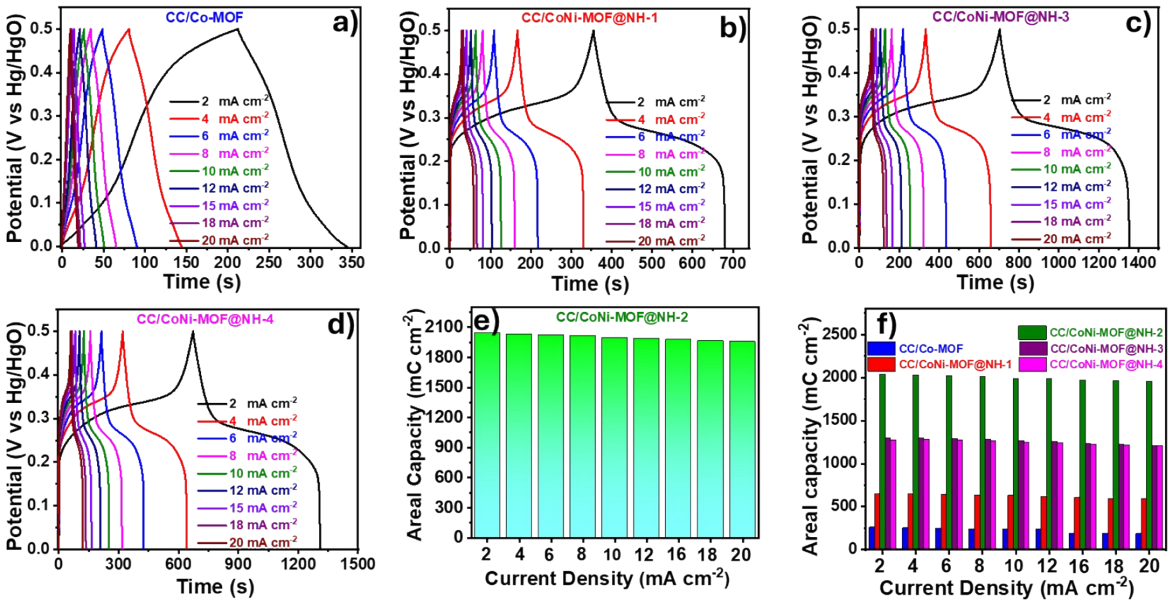

Figure S7. The GCD curves of (a) CC/Co-MOF, (b) CC/CoNi-MOF@NH-1, (c) CC/CoNi-MOF@NH-3, and (d) CC/CoNi-MOF@NH-4 electrodes at different current densities (2-20 mA cm^{-2}), (e) The variation of areal capacitance (C_a) values of CC/CoNi-MOF@NH-2 electrode at different current densities (2-20 mA cm^{-2}), and (f) The variation of areal capacity (C_a) values for CC/Co-MOF, CC/CoNi-MOF@NH-1, CC/CoNi-MOF@NH-2, CC/CoNi-MOF@NH-3, and CC/CoNi-MOF@NH-4 electrodes at different current densities (2-20 mA cm^{-2}).

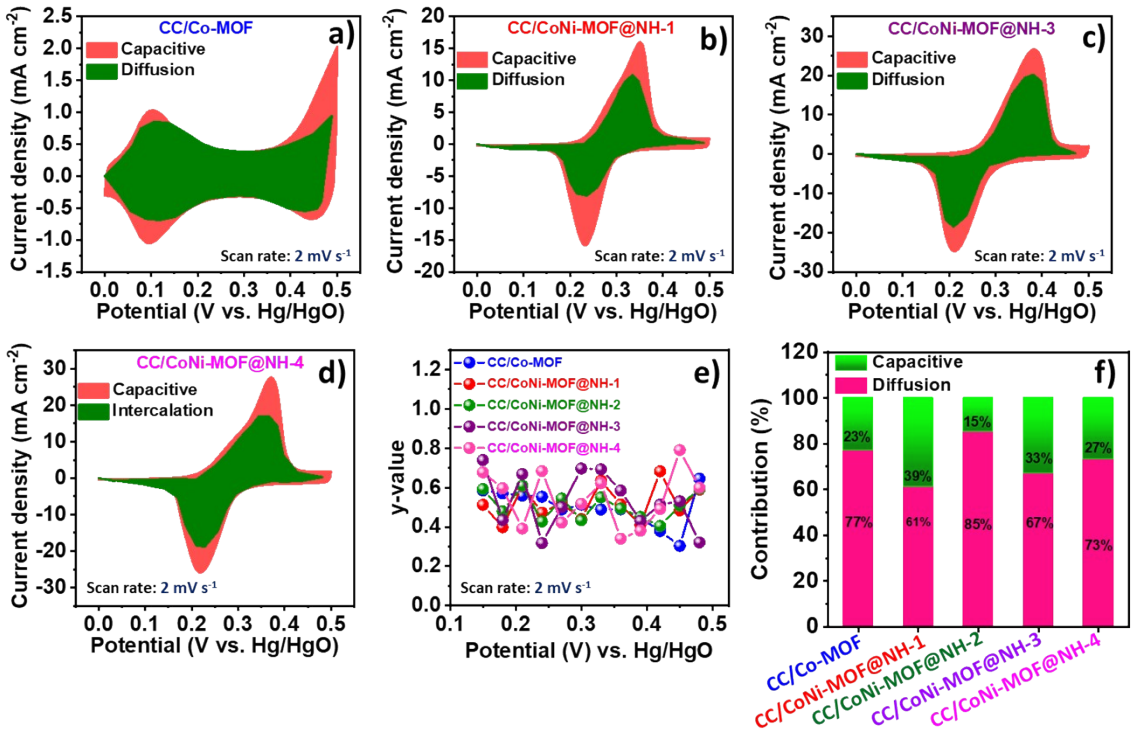

Figure S8. Capacitive and diffusion-controlled contribution fractions at the scan rate of 2 mV s^{-1} for (a) CC/Co-MOF, (b) CC/CoNi-MOF@NH-1, (c) CC/CoNi-MOF@NH-3, and (d) CC/CoNi-MOF@NH-4 electrodes, (e) Plot between the Y-value vs potential (V) (vs Hg/HgO) and (f) Percentage of capacitive and diffusion-controlled contributions for CC/Co-MOF, CC/CoNi-MOF@NH-1, CC/CoNi-MOF@NH-2, CC/CoNi-MOF@NH-3, and CC/CoNi-MOF@NH-4 electrodes at a scan rate of 2 mV s^{-1}.

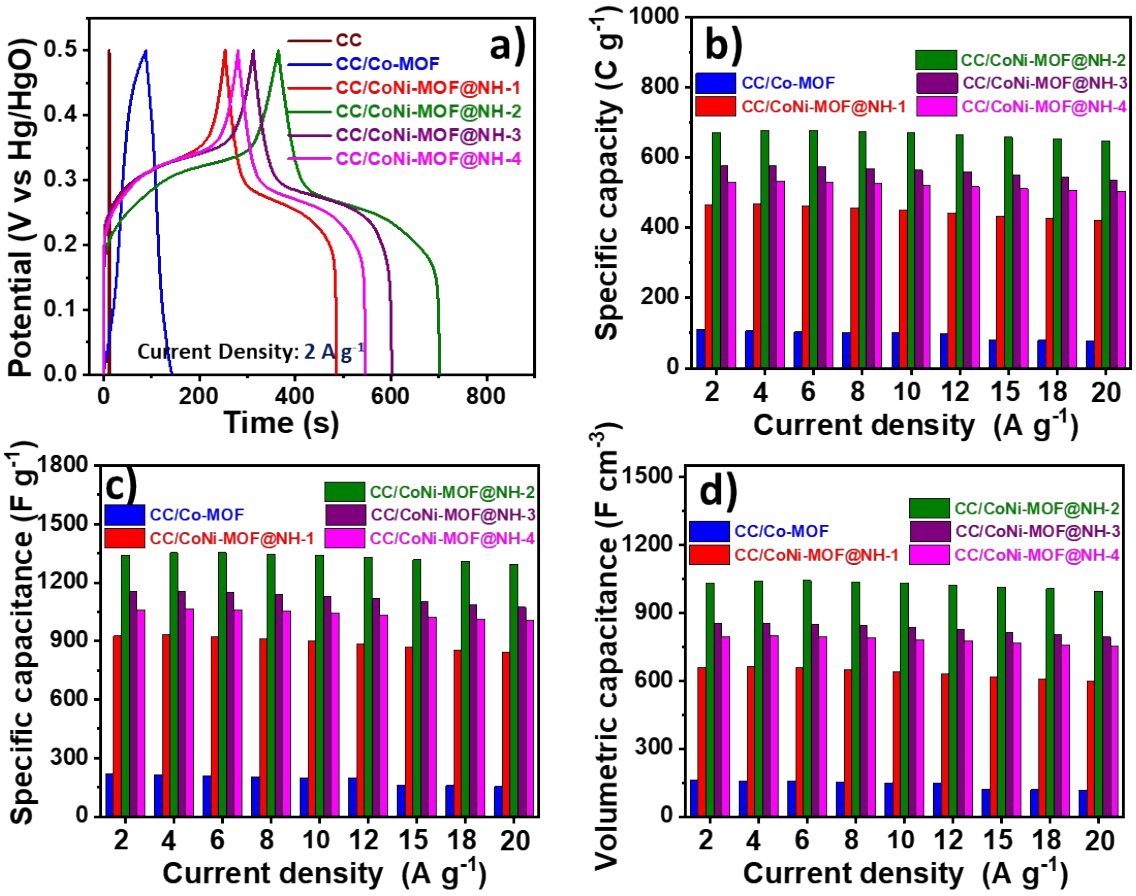

Figure S9. (a) Comparative GCD profiles of bare CC, CC/Co-MOF, CC/CoNi-MOF@NH-1, CC/CoNi-MOF@NH-2, CC/CoNi-MOF@NH-3, and CC/CoNi-MOF@NH-4 electrodes at a current density of 2 A g^{-1}, the variation of (b) Specific capacity (C_s), (c) Specific capacitance (C_{sp}), and (d) Volumetric capacitance (C_{vc}) values for CC/Co-MOF, CC/CoNi-MOF@NH-1, CC/CoNi-MOF@NH-2, CC/CoNi-MOF@NH-3, and CC/CoNi-MOF@NH-4 electrodes at different current densities (2-20 A g^{-1}).

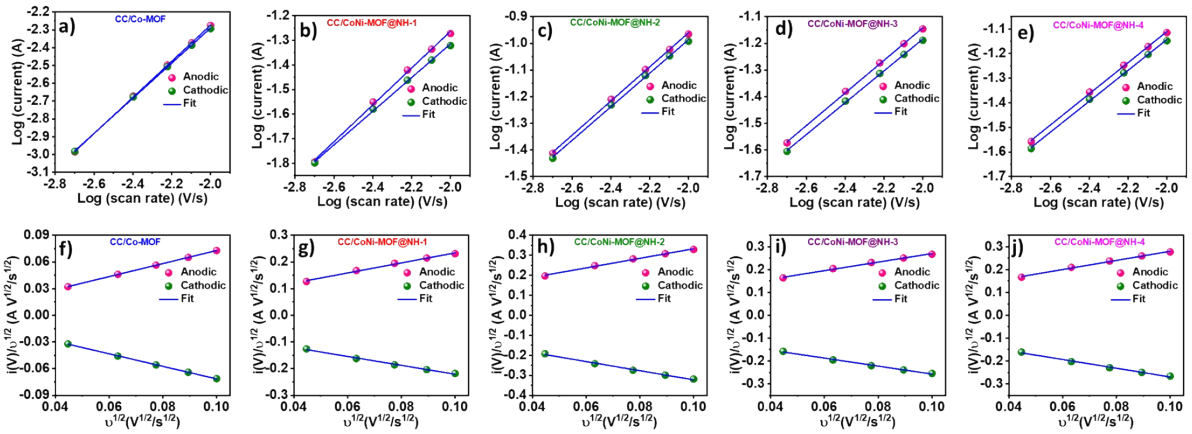

Figure S10. Logarithm profile of log(i) versus log (υ) for anodic and cathodic peaks at different potentials for (a) CC/Co-MOF, (b) CC/CoNi-MOF@NH-1, (c) CC/CoNi-MOF@NH-2, (d) CC/CoNi-MOF@NH-3, and (e) CC/CoNi-MOF@NH-4 electrodes and the graph between $i(V)/\upsilon^{1/2}$ and $\upsilon^{1/2}$ for (f) CC/Co-MOF, (g) CC/CoNi-MOF@NH-1, (h) CC/CoNi-MOF@NH-2, (i) CC/CoNi-MOF@NH-3, and (j) CC/CoNi-MOF@NH-4 electrodes.

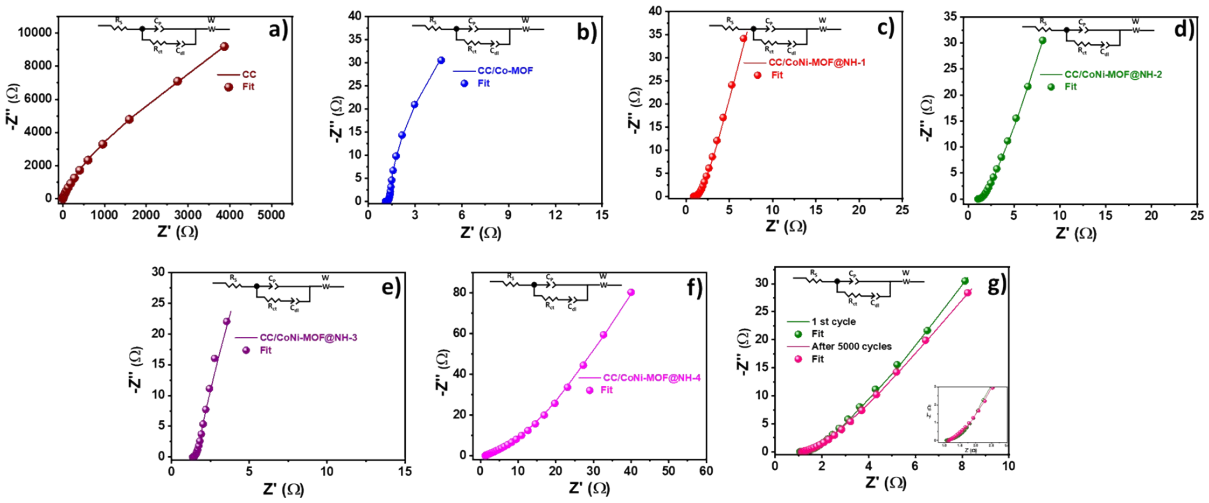

Figure S11. Nyquist plots fitted with equivalent circuits for (a) Bare CC, (b) CC/Co-MOF, (c) CC/CoNi-MOF@NH-1, (d) CC/CoNi-MOF@NH-2, (e) CC/CoNi-MOF@NH-3, (f) CC/CoNi-MOF@NH-4, electrodes and (g) CC/CoNi-MOF@NH-2 electrode before and after 5000 charge/discharge cycles, with the insets showing the respective magnified view.

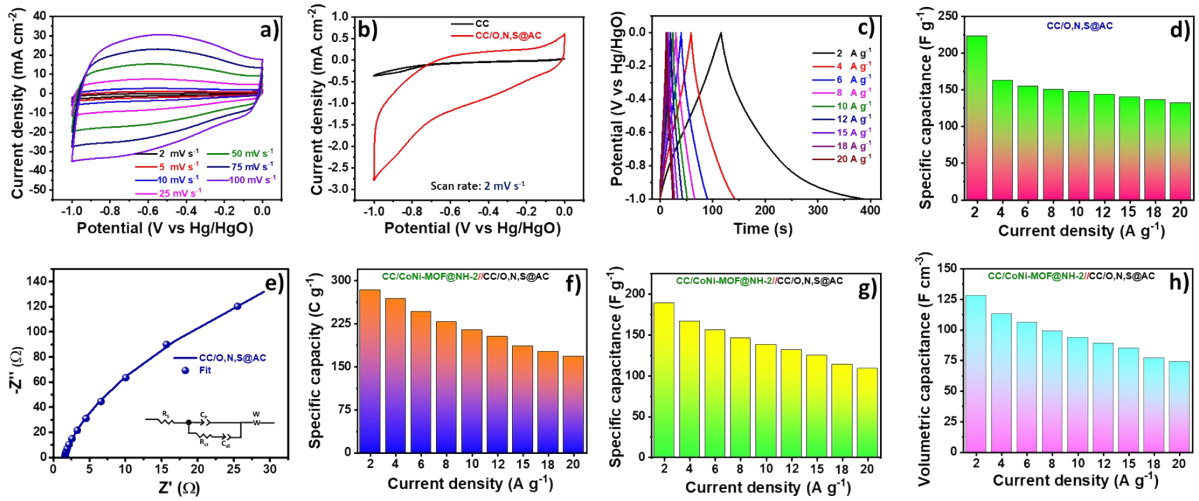

Figure S12. (a) CV curves of the negative electrode (CC/O,N,S@AC) at different scan rates (2-100 mV s^{-1}), (b) Comparison of CV curves of the negative electrode (CC/O,N,S@AC) and bare CC at a scan rate of 2 mV s^{-1} (c) GCD curves for CC/O,N,S@AC electrode at different current densities (2-20 A g^{-1}), (d) Comparison of specific capacitance (C_s) obtained from the GCDs of CC/O, N, S@AC electrode at different current densities (2-20 A g^{-1}), (e) Nyquist plot of CC/O, N, S@AC electrode and the inset shows the equivalent circuit, The variation of (f) Specific capacity (C_s), (g) Specific capacitance (C_{sp}), and (h) Volumetric capacitance (C_{vc}) values for the HSC (CC/CoNi-MOF@NH-2//CC/O, N, S@AC) at different current densities (2-20 A g^{-1}).

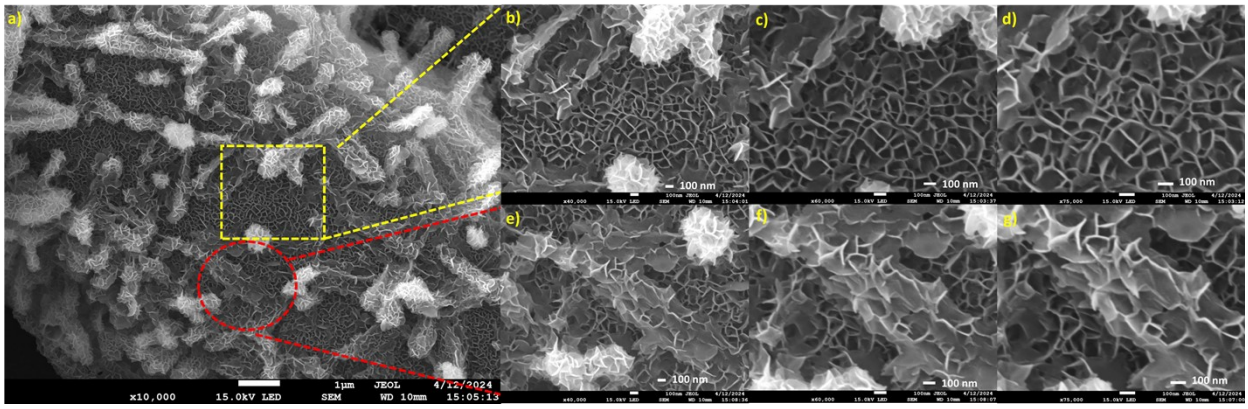

Figure S13. Post-mortem SEM analysis of CC/CoNi-MOF@NH-2 electrode after 10,000 continuous charge/discharge cycles at different places with various magnifications.